Numerical simulation of mechanical behavior of Zr-Nb alloys in a wide temperature range

†Vladimir A. Skripnyak[1], Evgeniya G. Skripnyak[1], VladimirV. Skripnyak[1], Vitas A. Serbenta[1], and Natalia V. Skripnyak[1]

[1]Research Laboratory of Properties of Substances in Extreme States, National Research Tomsk State University, Russia

*Presenting author: skrp@ftf.tsu.ru
†Corresponding author: skrp@ftf.tsu.ru

Abstract

The aim of this work was the evaluation of temperature and strain rate on the mechanical behavior of the zirconium-niobium alloys. This paper presents results on modelling and theoretical prediction of mechanical and deformation properties of Zr-Nb in a wide range of strain rates and temperature. Mechanical behavior of Zr–1 % Nb was numerically simulated using Johnson–Cook, and Zerilli –Armstrong constitutive equations. Material parameters of these constitutive equations were determined for Zr–1 % Nb alloys (E110). The numerical results on dynamic and quasi-static deformation of Zr−1 % Nb alloy are good agreed with experimental data. Strain rate sensitivity of the yield stress of Zr–Nb alloys at fixed temperature depends on the concentration of Nb, and parameters of grain size distribution. It is shown that the resistance to plastic deformation of Zr–Nb alloys is different under compression and tension at high-strain rates.
The results can be used in engineering analysis of designed technical systems for nuclear reactors.

Keywords: **Computer simulation, mechanical behavior, ductility, zirconium-niobium alloys, high strain rate, temperature**

Introduction

Improvement of technology of fabrication of fuel claddings and some constructional elements of nuclear reactors is connected with computer simulation of mechanical properties and structural evolution of radiation-resistant alloys Zr–Nb [1]. In this regard, there is an increasing need to develop computational models of the mechanical behaviour of advanced Zr-Nb in loading conditions close to operating ones. The Zr–Nb has a unique complex of physical and mechanical properties and is considered as promising structural alloys for nuclear reactors of IV generation. Coarse grained (CG) and ultrafine grained (UFG) zirconium alloys with a concentration of Nb below 2.5 weight % and additionally doped with Mo, Fe, Cr for the stabilization of precipitations of beta-phase Zr were studied during last decade [2]-[4]. It is known that the formation of ultrafine-grained structures in the alloys of Zr–Nb not only improves the yield and strength of the alloy, but also prevents the formation of cracks at the mesoscopic level [5]-[6]. In this connection, the mechanical behavior of Zr–Nb alloys was studied by numerical simulation method in the practically important temperature range from 297 K to 1243 K.

1 Material and samples

Mechanical behavior of ultrafine –grained (UFG) and coarse grained (CG) zirconium E110 (Zr-1%Nb) alloy was studied under tension at room temperature. Ultrafine grained specimens

of E110 alloy were produced by the severe plastic deformation method [7]. Sizes of specimens are shown in Table 1.

Table 1. Sizes of specimens of E100 (Zr-1%Nb) alloy

Coarse grained E110 alloy ($d_g^{(*)} \approx 55$ μm)			
Designation	Width of gage part of specimens (mm)	Thickness of specimens (mm)	Length of gage part of specimens (mm)
19	8.9±0.01	0.88±0.01	20.3±0.01
20	9.0±0.01	0.90±0.01	20.2±0.01
21	9.0±0.01	0.90±0.01	20.4±0.01
22	8.9±0.01	0.92±0.01	20.8±0.01
23	8.9±0.01	0.87±0.01	20.7±0.01
24	8.9±0.01	0.87±0.01	20.5±0.01
25	9.0±0.01	0.90±0.01	20.5±0.01
Ultrafine grained E110 (grain size $d_g \approx 0.5$ μm)			
26	9.0±0.01	0.90±0.01	20.5±0.01
27	9.0±0.01	0.90±0.01	20.3±0.01
28	9.0±0.01	0.85±0.01	20.3±0.01
29	8.9±0.01	0.90±0.01	20.5±0.01
30	9.0±0.01	0.90±0.01	20.5±0.01
31	9.0±0.01	0.90±0.01	20.5±0.01
32	8.9±0.01	0.90±0.01	20.5±0.01
33	8.9±0.01	0.90±0.01	20.3±0.01
34	9.0±0.01	0.90±0.01	20.7±0.01

$^{(*)}d_g$ is the grain size.

2 Quasistatic and dynamic tests

The tests were carried out at room temperature and strain rate 0.01 s^{-1} using the Instron test machine VHS 40/50-20 with a 50 kN load cell. The tensile force and displacement of the specimen were recorded at high temporal resolution up to complete fracture of the specimen. True strain and true stress at time moments of loading were determined by analytical relations [8]:

$$\varepsilon_1^{true} = \ln(1+\Delta l / l_0),\ \sigma_1^{true} = (F / A_0)(1+\Delta l / l_0), \quad (1)$$

where ε_1^{true} is true strain, σ_1^{true} is true stress, F is tensile force, A_0 is mean initial minimum cross sectional area of sheet sample, Δl, *and* l_0 are the elongation and the initial length of sample gage part.
True stresses and true strains were also determined by computer simulation.

3 Computational model

The computational model is based on the theoretical basis of continuum damage mechanics [9]. Mechanical behaviour was described by a system of conservation equations (mass, momentum and energy), kinematic equation and the constitutive equation. Initial and boundary conditions were added to the system of equations. The boundary conditions

correspond to the conditions of loading of the 3D body. Dog bone shape specimens were simulated under axial tension with a constant strain rate. The computer simulations were performed with the use of licensed AUTODYN software, and being a part of the package simulation of the dynamic loads of the package ANSYS WB 14.5. The calculations were carried out using solvers using finite-difference scheme of second order accuracy. The grid model of the samples used in tests is shown in Fig. 1.

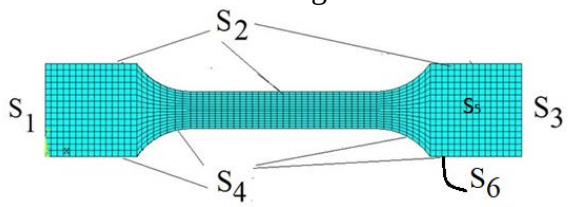

Figure 1. Grid model of flat sample

Boundary conditions corresponding to uniaxial tension of the sample at a constant strain rate have the form:

$$u_1|_{S_1}=0\ ,\ u_1|_{S_3}=0\ ;\ u_2|_{S_1}=0\ ,\ u_2|_{S_3}=V_2^{(0)};\ u_3|_{S_1}=0\ ,u_3|_{S_3}=0;\ \sigma_{ij}|_{S_2 US_4 US_5 US_6}=0, \quad (1)$$

where $u_i|_{S_j}$ are the components of the particle velocity vector on the surface S_j, v_{y_0} is the tensile velocity, σ_{ij} is the components of the stress tensor.

The initial conditions correspond to the free stress state of the material in a uniform temperature field.

$$\rho|_{t=0}=\rho_0\ ,\ \varepsilon_{ij}|_{t=0}=0,\ \sigma_{ij}|_{t=0}=0,\ T|_{t=0}=T_{test}\ , \quad (2)$$

where t is a time, ρ is a mass density, T_{test} is the initial temperature of specimen.

The flow stress of zirconium alloys under loading has been described using a modification of the Johnson-Cook model (3) and the Zerilli–Armstrong model (4) [8][10]. The flow stress of alloys has been described using a modification of the Johnson-Cook model (3) and the Zerilli–Armstrong model (4):

$$\sigma_s=\{A+B(\varepsilon_{eq}^P)^n+kd_g^{-1/2}\}[1+C\ln(\dot{\varepsilon}_{eq}/\dot{\varepsilon}_{eq0})]\{1-[\frac{T-T_0}{T_m-T_0}]^m\}, \quad (3)$$

where A, B, C, n, m, k are constants of material, d_g is the grain size, $\dot{\varepsilon}_{eq}=[(2/3)\dot{\varepsilon}_{ij}\dot{\varepsilon}_{ij}]^{1/2}$, $\dot{\varepsilon}_0=1.0s^{-1}$, $\varepsilon_{eq}^P=\int_0^t[(2/3)\dot{\varepsilon}_{ij}^P\dot{\varepsilon}_{ij}^P]^{1/2}dt$ is the plastic strain intensity, T is the temperature, T_0 is the room temperature, and T_m is the melting temperature.

Material constants of alloy the equation (3) of E110 (Zr−1% Nb) are given in Table 1.

Table 1. Material constants of modified Johnson-Cook model forE100 (Zr-1%Nb)

Coefficient / Zr-Nb alloy	A, GPa	B, GPa	n	k_g, GPa $nm^{1/2}$	C	m	T_m, K
E110	0,290	0,386	0,11	368 for 1.1 μm<dg<100 μm	0,14	0.6 at T< 1070 K 0.14 at T> 1070 K	1946

T_β is equal to 1070 K for Zr-1%Nb.

Updating of the constitutive equation of the Armstrong - Zerilli model can be written in the following form [10]:

$$\sigma_s = \sigma_{s0} + C_5(\varepsilon_{eq}^p)^{n_1} + k_{hp} d_g^{-1/2} + C_2 \exp\{-C_3 T + C_4 T \ln(\dot{\varepsilon}_{eq} / \dot{\varepsilon}_{eq0})\}. \quad (4)$$

where σ_{s0}, C_5, n_1, k_{hp}, C_2, C_3, C_4 are material coefficients.

Material coefficients of E110 (Zr−1% Nb) alloy are given in Table 2.

Table 2. Material parameter of the Armstrong-Zerilli model

Coefficient Zr−Nb alloy	σ_{s0}, GPa	k_{hp}, GPa nm$^{1/2}$	C_2, GPa	C_3, K^{-1}	C_4, K^{-1}	C_5, GPa	n_1
E110	0.110	368 for 1.1 μm<d_g<100 μm	1.015	8.77	3.95	4.05	0.19
(Zr−1%Nb)	0.445	40 for 0.08 μm<d_g<1.1 μm	1.015	10^{-3}	10^{-4}	10^{-3}	

Results and discussion

True stress versus true strain curves of E110 alloy are shown in Fig.2. The obtained data are in good agreement with the results [11]-[14].

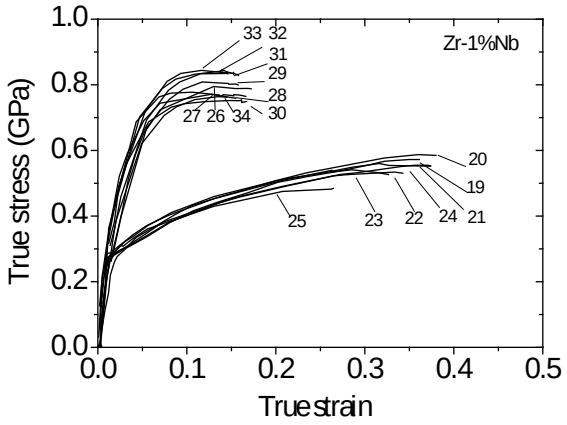

Figure 2. True stress versus true strain curves of ultrafine grained (curves 26-33) and coarse grained (curves 19-25) E100 (Zr-1%Nb) alloy under tension at 0.01 s^{-1} strain rate

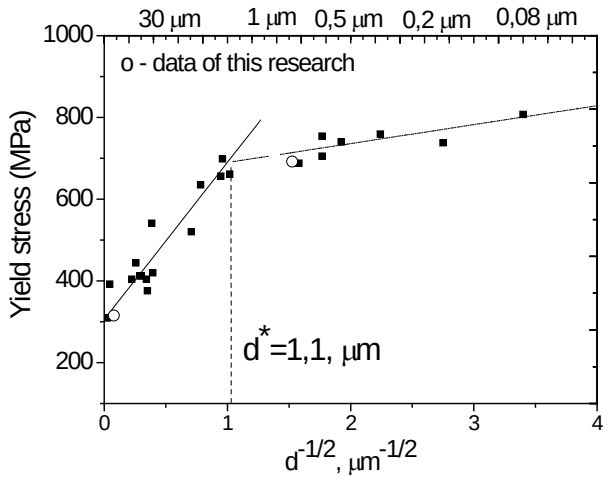

Figure 3. Yield stress versus grain size of zirconium alloys; symbols are experimental data [6][11]-[14]

The dependence of the yield stress on the grain size of coarse grained Zr−1%Nb alloys can be described by the Hall-Petch relation

$$\sigma_s = \sigma_{s0} + k_{hp} d_g^{-1/2}, \quad (5)$$

where σ_s is the yield strength, σ_{s0} and k_{hp} are parameters of material.
Parameters σ_{s0} and k_{hp} of zirconium-niobium alloys is equal to σ_{s0}= 322 MPa, k_{hp} = 368 MPa μm½, when grain size is in the range 1.1 μm < d_g < 100 μm. The values of σ_{s0} and k_{hp} change to σ_{s0} = 652 MPa, k_{hp} = 40 MPa·μm½ for alloys with grain size in the range of 0.08 μm < d < 1.1 μm. These parameters were used for numerical simulation.
Numerical values of σ_{s0} and k_{hp} depend on distribution of grain sizes [15]−[17].
Fig. 4(a) shows the calculated stress versus equivalent plastic strain curves for uniaxial tension of Zr−1%Nb−1%Sn alloy (E110) at strain rate of 10^{-3} s^{-1}.

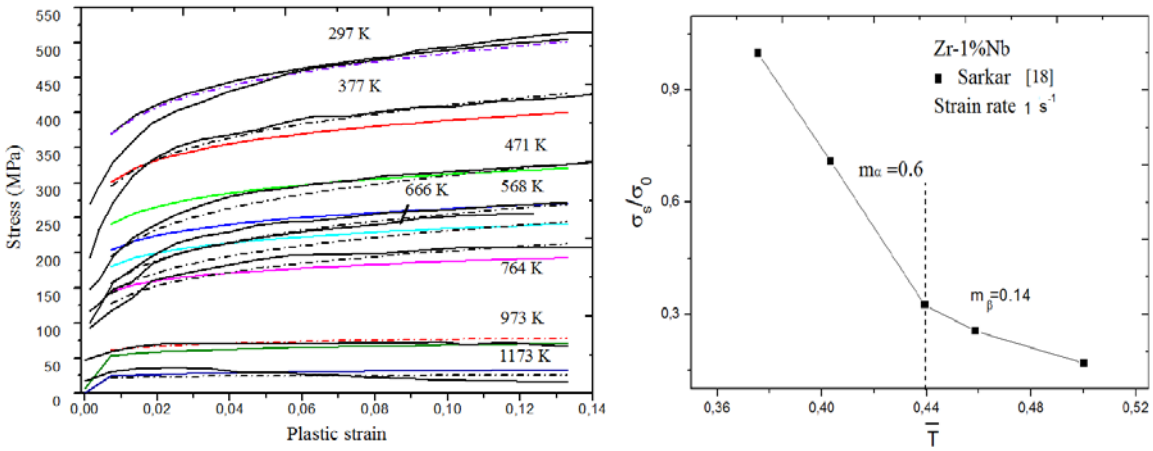

(a) (b)

Figure 4. (a) Stress versus plastic strain under uniaxial tension of Zr-1Nb-1Sn alloy at the strain rate of 10^{-3} s^{-1}; (b) normalized yield strength versus normalized temperature of Zr-1%Nb alloy at strain rate 1 s^{-1} (b). Symbols are experimental data [18]

Solid black curves indicate experimental true stress versus true strain [2]-[3]. Colored and dashed curves were obtained using equation (4) and (3), respectively. Results of simulation good agree with experimental data within temperature range from 297 K to 1173 K [2]-[3][18][19]. The constitutive equation (4) describes the change of the strain hardening in the temperature range more adequately in comparison with the constitutive equation (3).
The dependence of the normalized yield strength of alloy Zr−1% Nb under tension with a strain rate of 1 s^{-1} on the normalized temperature $\bar{T} = (T - T_r)/(T_m - T_r)$ is shown in Fig. 4(b).
The change of the curve slop σ_s/σ_{s0} ($\bar{T}$) at $\bar{T}$ =0.44 (T= ~1070K) is the result of a phase transition in Zr–1% Nb alloys. Phase transition from alpha phase (HCP lattice) to the beta phase (BCC lattice) depends on concentration of niobium.
Numerical means of m or C_3, in constitutive equations (3) and (4) are changed if the temperature exceeds the temperature of beginning of phase transformations, α → β (~ 1070 K).
Fig. 5 shows calculated yield strength versus logarithm of normalized strain rate under tension of the Zr–Nb. The average grain size was 15 μm. Solid curves calculated at temperatures from 295 K to 1273 K and strain rates from 10^{-3} s^{-1} to 10^{2} s^{-1}. The dashed curve calculated at the room temperature, and range of strain rates from 10^{-3} to 10^{6} s^{-1}. Experimental data [4][18]-[19] are shown by filled symbols. Thus, it was shown that the dependence of the yield strength of the Zr–1%Nb alloy on the logarithm of normalized strain rate is close to linear in the temperature range from 297 K to 1273 K and strain rates from 10^{-3} to 10^{2} s^{-1}.

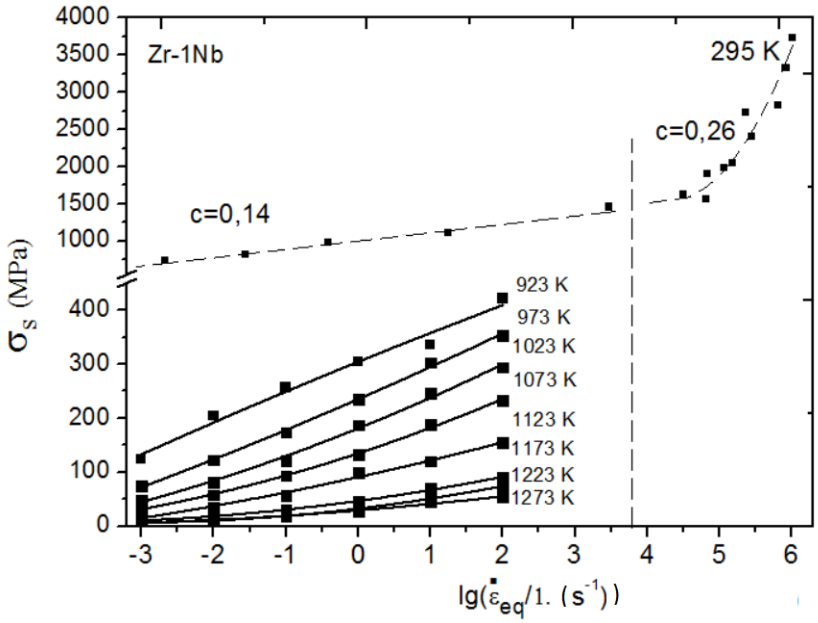

Figure 5. Normalized yield strength versus logarithm of normalized strain rate under tension for the samples of the Zr-1%Nb alloy; symbols are experimental data [4][18]-[19]

Both models (Zerilli–Armstrong and Johnson–Cook) allow obtaining satisfactory predictions of the yield stress under tension in the range of strain rates from 10^{-3} to ~10^{3} s^{-1} and temperature from 297 K to 1273 K. It was found, that it is necessary to change the numerical value of the coefficient c in the model of Johnson-Cook to obtain a satisfactory agreement of calculated yield strength of with experimental data [18]-[19]. Calculated stress – strain curves of Zr–1Nb under tension and compression and calculated stress versus equivalent plastic strain of UFG and CG Zr–1Nb is shown in Fig. 6 (a) and (b), respectively. Results of simulation is showed that the macroscopic flow stress of Zr–Nb alloys under dynamic compression and tension are various (See Fig.6(a)). This effect is caused by instabilities of plastic flow of Zr–1%Nb at the macro–and meso– scale levels under quasi-static and dynamic loads.

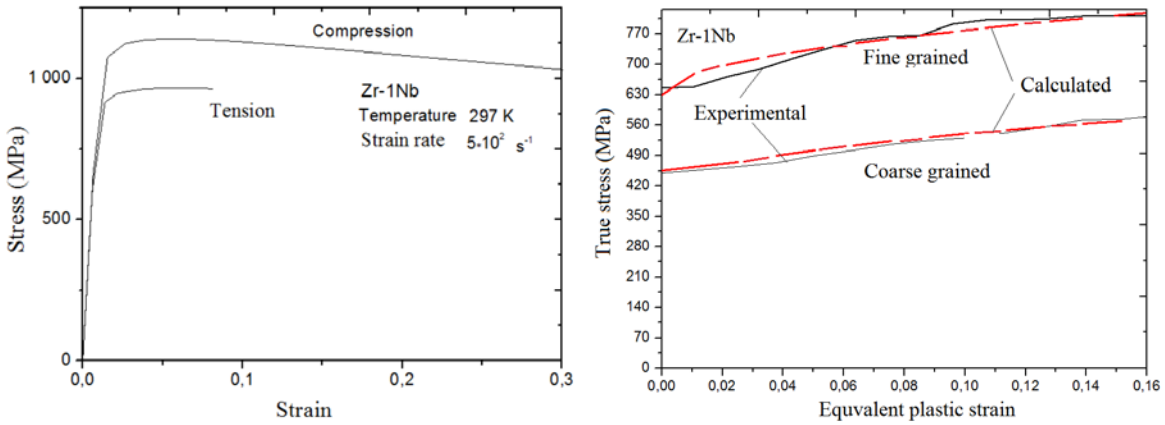

(a) (b)

Figure 6. (a) Calculated stress versus strain curves of Zr–1%Nb under tension and compression; (b) calculated stress versus equivalent plastic strain of UFG and CG Zr-1%Nb (b); solid curves are experimental data [5]; dashed curves are calculations by the Zerilli–Armstrong model

Results of numerical simulation showed decreasing of the yield stress under shear bands origin. Calculated stress – strain curves for CG and UFG specimens of the alloy E110 (Zr–1%Nb) at room temperature are shown in Figure 6 (b). The calculated yield stresses of ultrafine-grained Zr-1%Nb alloys are in good agreement with the experimental data due to using bilinear relation (5).

Conclusions

Mechanical behavior of ultrafine-grained and coarse grained Zr–Nb alloys was studied by experimental and computer simulation methods.

Experimental true stress versus true strain curves of E110 (Zr-1%Nb) alloy were obtained at room temperature.

Modified Zerilli–Armstrong and Johnson–Cook constitutive equations were used for numerical simulation of response of specimens under tension and compression.

Modifications of both models allow obtaining satisfactory predictions of the yield stress under tension within the range of strain rates from 10-3 to ~103 s-1 and temperature from 297 K to 1273 K.

It was shown that the dependence of normalized yield strength of Zr-1%Nb on normalized temperature can be approximated by a bilinear relation. The bilinear relation is due to change of mechanical properties of alloy caused by phase transition $\alpha \rightarrow \beta$ (T~ 1070 K) in Zr– 1%Nb alloys.

Acknowledgement

This work was supported partially by the Grant from the President of Russian Federation MK-2690.2017.8 and by The Tomsk State University competitiveness improvement programme. The authors are grateful to Professor Y. V. P. Sharkeev and researcher O. A. Belyavskaya for useful discussions and cooperation in experimental studies of alloys.

References

[1] Blokhin D. A., Chernov V. M., Blokhin A. I. (2011) Nuclear and physics properties of zirconium alloys E-110 and E-635 under long time neutron irradiation in the VVER-1000 reactor *Advanced materials*, № 5 23–29.
[2] Fong R. W. L. (2013) Anisotropic deformation of Zr–2.5Nb pressure tube material at high temperatures *Journal of Nuclear Materials*, **440** 467–476.
[3] Kapoor R., Wadekar S. L., Chakravartty J. K. (2002) Deformation in Zr–1Nb–1Sn–0.1Fe using stress relaxation technique *Materials Sci. and Eng*. A. **328** 324–333.
[4] Xiao D., Li Y., Hu S. (2010)High Strain Rate Deformation Behavior of Zirconium at Elevated Temperatures *Journal of Materials Science & Technology* **26** 878-882.
[5] Stepanova E. N., Grabovetskaya G. P. (2015) Effect of hydrogen on the structural and phase state and the deformation behavior of the ultrafine-grained Zr–1Nb alloy *Journal of Alloys and Compounds* **645** 271–274.
[6] Cao W.Q., Yu S.H., Chun Y.B. (2005) Strain path effects on the microstructure evolution and mechanical properties of Zr702 *Materials Sciences and Engineering A.* **395** 77–86.
[7] Sharkeev Y. P., Eroshenko A. Y., Kulyashova K. S. (2013) Microstructure, mechanical and biological properties of zirconium alloyed with niobium after severe plastic deformation *Material wissenschaft und Werkstofftechnik* **44** 198-204.
[8] Valoppi B., Bruschi S., Ghiotti A., Shivpur R. (2017) Johnson-Cook based criterion incorporating stress triaxiality and deviatoric effect for predicting elevated temperature ductility of titanium alloy sheets, *International Journal of Mechanical Sciences* **123** 94-105.

[9] Zhang W., Cai Y. Continuum Damage Mechanics and Numerical Applications. *Springer Science & Business Media, 2010 - Technology & Engineering*, 1000 p.
[10] Zerilli F.J., Armstrong R.W. (1992) The effect of dislocation drag on the stress-strain behaviour of F.C.C. metals, *Acta Metall. Mater* **40** 1803–1808.
[11] Kondo R., Nomura N., Suyalatu, Tsutsumi Y., Doi H., Hanawa T. (2011) Microstructure and mechanical properties of as-cast Zr–Nb alloys *Acta Biomaterialia* **7** 4278–4284.
[12] Ruestes C.J., Bertolino G., Ruda M. (2014) Grain size effects in the deformation of [0001] textured nanocrystalline Zr, *Scripta Materialia* **71** 9–12
[13] Guo D., Zhang Z., Zhang G., Li M., Shi Y., Ma T., Zhang X. (2014) An extraordinary enhancement of strain hardening in fine-grained Zirconium *Materials Sciences and Engineering A.* **591** 167–172.
[14] Jiang L., Perrez-Prado M.T., Gruber P.A. (2008) Texture, microstructure and mechanical properties of equiaxed ultrafine-grained Zr fabricated by accumulative roll bonding// Acta Materialia **56** 1228–1242.
[15] Skripnyak V. A. and Skripnyak E. G. (2017) *Mechanical behaviour of nanostructured and ultrafine-grained metal alloy under intensive dynamic loading*, Chapter 2: *Nanotechnology and Nanomaterials» "Nanomechanics"*, Eds.by A. Vakhrushev, ISBN 978-953-51-3182-3, Print ISBN 978-953-51-3181-6, 2017. DOI: 10.5772/Intech open. 68291.
[16] Skripnyak V.A., Skripnyak N.V., Skripnyak E.G., Skripnyak V.V. (2017) Influence of grain size distribution on the mechanical behavior of light alloys in wide range of strain rates, *AIP Conference Proceedings*, 1793, art. No. 110001.
[17] Skripnyak N.V., Skripnyak E.G., Skripnyak V.A., Skripnyak V.V., Vaganova I.K. (2014) Failure mechanisms of light alloys with a bimodal grain size distribution *11th World Congress on Computational Mechanics, WCCM 2014, 5th European Conference on Computational Mechanics, ECCM 2014 and 6th European Conference on Computational Fluid Dynamics, ECFD*, 3915-392.
[18] Sarkar A., Chandanshive S. A., Thota K. M. (2017) High temperature deformation behavior of Zr-1Nb alloy *Journal of Alloys and Compounds* **703** 56-66.
[19] Kazakov D. N., Kozelkov O. E., Mayorova A. S. (2015) Dynamic behavior of zirconium alloy E110 under sub microsecond shock-wave loading *EPJ Web of Conferences* **94** 1–5.